JACS
JOURNAL OF THE AMERICAN CHEMICAL SOCIETY

ARTICLE

pubs.acs.org/JACS

Scaffolding, Ladders, Chains, and Rare Ferrimagnetism in Intermetallic Borides: Electronic Structure Calculations and Magnetic Ordering

Jakoah Brgoch,[†] Christian Goerens,[‡] Boniface P. T. Fokwa,[‡] and Gordon J. Miller*[,†]

[†]Department of Chemistry, Iowa State University, Ames, Iowa 50011, United States

[‡]Institute of Inorganic Chemistry, RWTH-Aachen University, Landoltweg 1, D-52056 Aachen, Germany

Supporting Information

ABSTRACT: The electronic structures of "$Ti_{9-n}Fe_{2+n}Ru_{18}B_8$" ($n$ = 0, 0.5, 1, 2, 3), in connection to the recently synthesized $Ti_{9-n}Fe_{2+n}Ru_{18}B_8$ (n = 1, 2), have been investigated and analyzed using LSDA tight-binding calculations to elucidate the distribution of Fe and Ti, to determine the maximum Fe content, and to explore possible magnetic structures to interpret experimental magnetization results. Through a combination of calculations on specific models and using the rigid band approximation, which is validated by the DOS curves for "$Ti_{9-n}Fe_{2+n}Ru_{18}B_8$" ($n$ = 0, 0.5, 1, 2, 3), mixing of Fe and Ti is anticipated at both the 2b- and 4h-chain sites. The model "$Ti_{8.5}Fe_{2.5}Ru_{18}B_8$" ($n$ = 0.5) revealed that both Brewer-type Ti−Ru interactions as well as ligand field splitting of the Fe 3d orbitals regulated the observed valence electron counts between 220 and 228 electrons/formula unit. Finally, models of magnetic structures were created using "$Ti_6Fe_5Ru_{18}B_8$" (n = 3). A rigid band analysis of the LSDA DOS curves concluded preferred ferromagnetic ordering at low Fe content ($n \leq 0.75$) and ferrimagnetic ordering at higher Fe content ($n > 0.75$). Ferrimagnetism arises from antiferromagnetic exchange coupling in the scaffold of Fe1-ladder and 4h-chain sites.

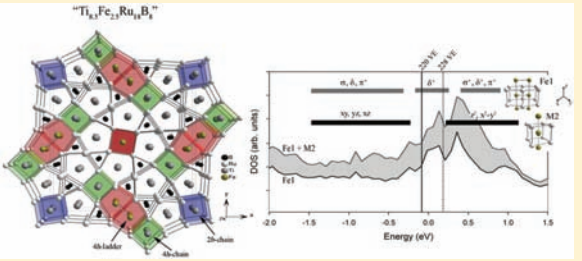

INTRODUCTION

In the past two decades a class of complex intermetallic borides has been synthesized containing magnetically active 3d atoms in close proximity to each other, allowing for studies of magnetic exchange as a function of valence electron count.[1−4] Some of these compounds are variants of the $Zn_{11}Rh_{18}B_8$-type structure, which crystallizes in the *P4/mbm* (no. 127) space group. Substitution of zinc by both titanium and iron, along with replacing rhodium with ruthenium, leads to the previously reported compound $Ti_9Fe_2Ru_{18}B_8$.[5] This structure contains 'ladders' of iron atoms where the 'rungs' are formed by Fe-dimers with an interatomic distance of ca. 2.5 Å and separated by ca. 3.0 Å along the [001] direction. The distances are short enough for through-space magnetic exchange to occur; as a result, the magnetic properties of this compound were investigated both experimentally and theoretically.[5]

$Ti_9Fe_2Ru_{18}B_8$ was determined to order ferromagnetically with a magnetic moment of 1.2 μ_B at 7 T and a Curie temperature (T_C) of 200 K. The Weiss constant (θ) is approximately +290 K, further indicating a strong (Fe−Fe) ferromagnetic exchange interaction.[5] The magnetic ordering was also predicted to be ferromagnetic by theory. An analysis of the crystal orbital Hamilton populations (−COHP) and the density of states (DOS) curves showed the occupation of Fe−Fe antibonding states and a local maximum in the nonmagnetic DOS at the Fermi level, both of which point toward electronic instability in the system.[6,7] Allowing the structure to relax through spin polarization resulted in the removal of both the Fe−Fe antibonding states and the peak in the DOS and effects ferromagnetic ordering along the rungs of the 'ladders'. A comparison of total energies among various magnetically ordered models confirmed ferromagnetic ordering to be preferred; e.g., the model with antiferromagnetic ordering along the [001] direction is 45.4 meV/formula unit above the ferromagnetic model. In these models, the 'rungs' of the ladder were treated as ferromagnetic stemming from a triplet spin state of neutral iron dimers in a D_{2h} crystal field.

Further addition of iron to this species, by replacing Ti according to $Ti_{9-n}Fe_{2+n}Ru_{18}B_8$ (n = 1, 2), has been synthesized and shows Fe-based 'ladders' as well as additional 'chains', about which the reader is referred to ref 8. These 'chains' are similar to those present in the isostructural $Zn_{10}FeRh_{18}B_8$ and the analogous $Sc_2Fe(Ru_{5-x}Rh_x)B_2$ (x = 0−5) and $Zr_2Fe_{1-\delta}(Ru_{1-x}Rh_x)_{5+\delta}B_2$ (δ = ca. 0.2, x = 0, 1).[1,3,4,9] The Fe atoms in the title structure partially substitute for Ti in the pseudocubic prisms at Wyckoff sites 2b and 4h. The 2b sites form chains along the [001] direction, well separated from the other sites occupied by 3d metals, whereas the 4h sites are ca. 3.0 Å from the Fe 'ladders'. The proximity of the 4h chains to the ladders can also be described as a tetramer of atoms that, when considered along the [001] direction, forms a 'scaffold' structure. Thus, direct

Received: February 7, 2011
Published: April 07, 2011

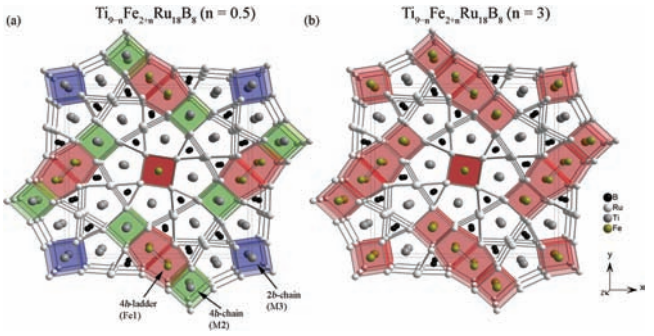

Figure 1. (a) "$Ti_{9-n}Fe_{2+n}Ru_{18}B_8$" ($n$ = 0.5) and (b) the fully occupied "$Ti_{9-n}Fe_{2+n}Ru_{18}B_8$" ($n$ = 3) shown as a perspective view along the [001] direction. The red polyhedra are occupied by Fe, the blue polyhedra are occupied by Ti in the 2b-chains, and the green polyhedra are occupied by Ti in the 4h-chains.

(through-space) magnetic exchange interactions between the 4h-chain and the 'ladder' can also be expected. Fe atoms occupying the 2b-chains are located ca. 6.5 Å from the 4h-chain and 7.9 Å from the 'ladder', a feature that could result in indirect (through-bond) exchange interactions but weaker through-space interactions. Therefore, the $Ti_{9-n}Fe_{2+n}Ru_{18}B_8$ (n = 1, 2) system provides an interesting platform for investigating various long-range magnetic ordering in intermetallic borides.

Here, we present a theoretical analysis of the electronic structures of "$Ti_{9-n}Fe_{2+n}Ru_{18}B_8$" ($n$ = 0, 0.5, 1, 2, 3), which represent the experimentally determined compounds $Ti_{9-n}Fe_{2+n}Ru_{18}B_8$ (n = 1, 2).[8] These analyses elucidate factors influencing the extent of Fe content as well as the ordering of 3d metals Ti and Fe among various crystallographic sites. Additionally, an investigation of magnetic structures stemming from preliminary experimental data for $Ti_{9-n}Fe_{2+n}Ru_{18}B_8$ (n = 1, 2) is undertaken through the development of a hypothetical "$Ti_6Fe_5Ru_{18}B_8$", i.e., n = 3 in $Ti_{9-n}Fe_{2+n}Ru_{18}B_8$, illustrated in Figure 1b, in which those sites occupied by Ti and Fe, i.e., the 2b and 4h positions, are fully occupied by Fe atoms. This hypothetical structure is electron rich as compared to all experimentally observed cases, so its density of states is integrated to the experimental valence electron (VE) range, 220−228 VE, via a rigid-band model in order to determine the preferred magnetic model.

ELECTRONIC STRUCTURE CALCULATIONS

The calculations of the electronic and magnetic structures were performed using the tight-binding, linear muffin-tin orbital method with the atomic-spheres approximation (TB-LMTO-ASA)[10,11] using the Stuttgart code.[12] Exchange and correlation were treated by the local density approximation (LDA) and the local spin density approximation (LSDA), which was parametrized according to von Barth and Hedin.[13] In the ASA method, space is filled with overlapping Wigner−Seitz (WS) spheres. The symmetry of the potential is considered to be spherical inside each WS sphere, and a combined correction is used to take into account the overlapping part. The corresponding WS radii are 1.53−1.58 Å (Ru), 1.67−1.72 Å (Ti), 1.43−1.44 Å (Fe), and 1.12 Å (B). Space-filling, empty spheres were necessary in all models, with five spheres present in the single crystallographic unit cell and ten spheres present in the doubled unit cell. All of the empty spheres have WS radii between 0.53 and 0.84 Å and are

Table 1. Substitution Patterns, Valence Electron (VE) Counts, And Space Groups Constructed for the Calculation of $Ti_{9-n}Fe_{2+n}Ru_{18}B_8$ (n = 0, 0.5, 1, 2, 3)

			$Ti_{9-n}Fe_{2+n}Ru_{18}B_8$: substitution pattern		
atom	VE count	space group	2b-chain (M3)	4h-chain (M2)	4h-ladder (Fe1)
n = 0	220	$P4/mbm$	Ti	Ti	Fe
n = 0.5	222	$P4/m$	Ti/Fe	Ti	Fe
n = 1	224	$P4/mbm$	Fe	Ti	Fe
n = 2	228	$P4/mbm$	Ti	Fe	Fe
n = 3	232	$P4/mbm$	Fe	Fe	Fe

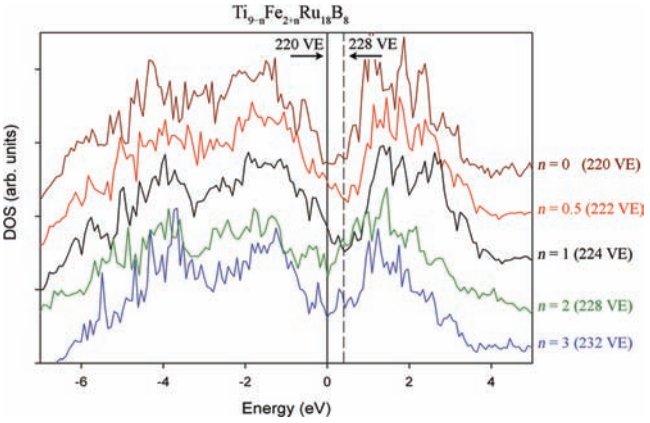

Figure 2. Total DOS curves for the $Ti_{9-n}Fe_{2+n}Ru_{18}B_8$ (n = 0, 0.5, 1, 2, 3) using LSDA. The reference energy (0 eV) is set to 220 VE; the dashed line is set to 228 VE. The DOS curves are offset for clarity.

clustered within the elongated hexagonal prism around the iron 'ladders'. Their locations are presented in Supporting Information.

The electronic structures of "$Ti_{9-n}Fe_{2+n}Ru_{18}B_8$" ($n$ = 0, 0.5, 1, 2, 3) were calculated using the tetragonal space groups $P4/mbm$ (no. 127), $P4/m$ (no. 83), and $P4$ (no. 75) as needed. The basis set of each calculation includes B (2s, 2p), Ru (5s, 5p, 4d), Ti (4s, 4p, 3d), and Fe (4s, 4p, 3d) wave functions. A mesh of 143 **k** points in the irreducible wedge of the first Brillouin zone was used to obtain all integrated values, including the density of states (DOS), integrated DOS (IDOS) values, which are valence electron counts, and crystal orbital Hamilton population (−COHP)[14] curves. To model antiferromagnetic ordering, a unit cell doubled along the [001] direction was created using space group $P4$ (no. 75). The magnetic ordering models were calculated using 54 **k** points.

RESULTS AND DISCUSSION

Several structural models were constructed to investigate theoretically the site preferences for Fe atoms, the maximum Fe content, the electronic structures, and possible magnetic ordering patterns in $Ti_{9-n}Fe_{2+n}Ru_{18}B_8$. These models of $Ti_{9-n}Fe_{2+n}Ru_{18}B_8$ include n = 0, 0.5, 1, 2, 3; their VE counts, space groups, and distributions of the 3d metal atoms (Fe and Ti) are listed in Table 1.

"$Ti_{9-n}Fe_{2+n}Ru_{18}B_8$" ($n$ = 0, 1, 2, 3) were all calculated using the space group, $P4/mbm$, placing the Fe atoms at the 2b- or 4h-chains to achieve the desired stoichiometry. "$Ti_{8.5}Fe_{2.5}Ru_{18}B_8$"

dx.doi.org/10.1021/ja200909r |J. Am. Chem. Soc. 2011, 133, 6832–6840

Table 2. Partial IDOS Values for the 2b-Chain ("Ti"), 4h-Chain ("Ti"), and 4h-Ladder ("Fe") between 220 and 228 VE Counts Obtained from the DOS of "$Ti_9Fe_2Ru_{18}B_8$"[a]

VE count	2b-chain (M3)	4h-chain (M2)	4h-ladder (Fe1)
220	4.39	4.31	8.28
222	4.42	4.33	8.58
224	4.44	4.35	8.84
228	4.46	4.39	9.53

[a] The WS radii, respectively, for Ti and Fe atoms are 1.62 Å and 1.45 Å.

(n = 0.5 case) was calculated in the subgroup $P4/m$ to allow the additional Fe atoms to replace Ti atoms in one-half of the 2b-chain sites of the parent $Ti_9Fe_2Ru_{18}B_8$. Lowering the symmetry from $P4/mbm$ to $P4/m$ splits numerous Wyckoff positions in the original crystal structure: (1) the 8i positions of the Ru net are reduced to two sets of 4j positions; (2) the 8j positions of Ti are split into two 4k positions; (3) the 8j positions of B are reduced to two 4k positions; (4) the 2b sites are lowered to a 1b and a 1d site. Among these, only the 2b sites exhibited mixed occupancy by Ti and Fe in the experimental $Ti_{9-n}Fe_{2+n}Ru_{18}B_8$ (n = 1, 2).[9] This splitting of the 2b site creates alternating ···Fe—Ti··· chains along the [001] direction and allows theoretical assessment of the atomic mixing at this chain site (see Figure 1a). "$Ti_{8.5}Fe_{2.5}Ru_{18}B_8$" ($n$ = 0.5), therefore, was constructed in this manner for three reasons: (1) to allow tetragonal symmetry to be maintained; (2) to place the additional Fe atoms in crystallographic sites satisfying the experimentally determined site preference; (3) to retain mixing of the 3d metal atoms for the 2b-chains.

The total DOS curves based on LSDA for the five cases "$Ti_{9-n}Fe_{2+n}Ru_{18}B_8$" ($n$ = 0, 0.5, 1, 2, 3), illustrated in Figure 2, show extensive similarities, which ratify using the rigid-band approximation for an interpretation of many experimental details (The DOS curves based on LDA are available in Supporting Information). The most notable features for each DOS curve include a pseudogap and VE counts that place the Fermi levels within this region of the DOS. Observed $Ti_{9-n}Fe_{2+n}Ru_{18}B_8$ phases exhibit VE counts between 220 and ca. 228 electrons, i.e., n = 0 and n = 2. The deepest pseudogaps occur for the n = 0, 0.5, and 1 models; they become shallow for n = 2, and then more distinguishable for the n = 3 case. As we will explain further in an examination of the model "$Ti_{8.5}Fe_{2.5}Ru_{18}B_8$" ($n$ = 0.5), the major peak below each pseudogap arises primarily from Ru 4d states, the major peak above each pseudogap originates from Ti 3d states, and Fe 3d states fall largely within each pseudogap. Thus, as the Fe content rises, and, thus, the Ti content drops, the pseudogaps become less distinct as Fe content, i.e., n, increases in the DOS curves of "$Ti_{9-n}Fe_{2+n}Ru_{18}B_8$". Spin polarization of the Fe 3d orbitals enhances the pseudogap in the DOS curve of "$Ti_6Fe_5Ru_{18}B_8$" (n = 3).

The Coloring of Ti and Fe Atoms at the 2b- and 4h-Chains. An important factor influencing the distribution of similar atomic species in a structure is minimizing both the site energies and bond energies for the atoms under consideration.[15] Computationally, one can also evaluate total electronic energies for various structural models for a fixed chemical composition. However, in TB-LMTO-ASA, these total energies are significantly dependent on the various Wigner—Seitz radii used for the different atoms and a less reliable method of interpretation. Therefore, to investigate factors affecting the distribution of Ti and Fe atoms at the 2b and 4h-chain sites of "$Ti_{9-n}Fe_{2+n}Ru_{18}B_8$," for which a rigid-band approximation is reasonable for $n \leq 3$. An analysis of the partial IDOS values (using LSDA) of these sites over the range of experimental VE counts[9] using "$Ti_9Fe_2Ru_{18}B_8$" as a model, with Ti atoms fully occupying the 2b and 4h-chain sites, was carried out and summarized in Table 2.

Although the IDOS values listed in Table 2 are also dependent on the WS radii, various radii values were examined, and those that produced the lowest total electronic energy of "$Ti_9Fe_2Ru_{18}B_8$" were analyzed. We carried out a similar analysis using "$Ti_6Fe_5Ru_{18}B_8$", with Fe atoms fully occupying the 2b- and 4h-chain sites. These results are qualitatively identical; the numerical results may be obtained in Supporting Information. The VE counts of these two chain sites, based on IDOS values, are similar in magnitude through the entire electron count range, with a slight preference for a more electron-rich element (Fe) to occupy the 2b-chain site over the entire range. However, the small differences in IDOS values (ca. 0.1 electron) for the 2b- and 4h-chain sites suggest that it will be difficult to differentiate fully the Ti/Fe site preferences experimentally.

An analysis of the results in Table 2 emphasize the site energy term in the total valence electron energy.[15] A comparison of the two local environments reveals differences in the second nearest neighbor shell of atoms. The 3d metal in both the 2b- and 4h-chains are surrounded by eight Ru nearest neighbors in a distorted cube and then by six Ti/Fe atoms in the second shell. This second shell of atoms surrounding each 2b site includes four Ti atoms in the equatorial ab-plane and then the other 2b-site atoms along the c-direction. For the 4h sites, the equatorial ab-plane has three Ti and one Fe second nearest neighbor (see Figure 1a). Thus, on the basis of site energies, the 2b-chain prefers a Fe content higher than that of the 4h-chain because the 2b site is surrounded by more electropositive metals. However, these neighboring sites also engage in orbital interactions, which contribute to the bond energy term that can also influence atomic distributions. Table 3 summarizes an analysis of integrated −COHP (−ICOHP) values for nearest and next nearest neighbor contacts at the 2b-chain (M3) and 4h-chain (M2) when they are occupied by either Fe or Ti for "$Ti_{9-n}Fe_{2+n}Ru_{18}B_8$". The total −ICOHP value for each atom(site) entry summed over all neighboring interactions is also given. In both sites, this sum is greater for Ti than for Fe, but the difference of these values is greater at the 2b-chain (M3) site than at the 4h-chain (M2) site. This result suggests that, due to bond energies, there is a greater energetic preference for Ti atoms to occupy the 2b-chain site than Fe.

Thus, an analysis of the coloring of Ti and Fe atoms at the crystallographically distinct chains, 2b (M3) and 4h (M2) sites, reveals competing and opposing tendencies for the atomic distribution. The experimentally assessed site preference[9] concluded a statistical distribution, which would be in line with the competition between the resulting competition between site energy and bond energy influences. On the other hand, within two standard deviations, one might conclude a slight preference for Fe to occupy the 2b-chains over the 4h-chains,[8] for which the site energy, which is dictated by the potential set up by the structural environment, exerts a slightly greater effect than the just the neighboring orbital interactions.

"$Ti_{8.5}Fe_{2.5}Ru_{18}B_8$" Electronic Structure. In summary, both site energy and bond energy terms affect the distribution of Fe and Ti atoms on the 3d metal sites, i.e., 2b-chains and 4h-chains. Although the refined composition from single crystal analysis for

Table 3. −ICOHP Values for Nearest and Next Nearest Neighbor Contacts at the 2b-Chain (M3) and 4h-Chain (M2) Sites in "$Ti_{9-n}Fe_{2+n}Ru_{18}B_8$" ($n$ = 1, 2)

atom (site)	contact	distance (Å)	no.	−ICOHP (eV/bond)	total −ICOHP (eV)
Fe(2b)-	Ru	2.575	8×	1.917	15.336
	Ti	3.338	4×	0.519	2.076
	Fe[001]	2.968	2×	0.792	1.584
				summed −ICOHP =	18.996
Ti(2b)-	Ru	2.575	8×	2.094	16.752
	Ti	3.338	4×	0.626	2.504
	Ti[001]	2.968	2×	0.907	1.814
				summed −ICOHP =	21.070
Fe(4h)-	Ru	2.575	4×	1.905	7.620
	Ru	2.576	4×	2.021	8.084
	Ti	3.259	1×	0.598	0.598
	Ti	3.435	2×	0.512	1.024
	Fe	3.033	1×	0.775	0.775
	Fe[001]	2.968	2×	0.756	1.512
				summed −ICOHP =	19.613
Ti(4h)-	Ru	2.575	4×	2.072	8.288
	Ru	2.576	4×	2.223	8.892
	Ti	3.259	1×	0.704	0.704
	Ti	3.435	2×	0.388	0.776
	Fe	3.033	1×	0.658	0.658
	Ti[001]	2.968	2×	0.894	1.788
				summed −ICOHP =	21.106

one Fe-rich specimen is $Ti_{8.1(1)}Fe_{2.9}Ru_{18}B_8$ (223.6 VE), mixed Ti/Fe occupancies are refined at both the 2b and 4h sites.[8] Given the slight preference for Fe atoms in the 2b site, the hypothetical "$Ti_{8.5}Fe_{2.5}Ru_{18}B_8$" ($n$ = 0.5; 222 VE) was constructed to examine its electronic structure and gain insights about the maximum Fe content. The total DOS and the atomic partial DOS curves using LDA, presented as DOS/atom, are shown for "$Ti_{8.5}Fe_{2.5}Ru_{18}B_8$" in Figure 3, with the Fermi levels associated with the range of VE counts, i.e., 220−228 VE, noted. The reference energy of these curves is the Fermi level for 222 VE. A broad "pseudogap", which spans states integrating between 195 VE (−0.9 eV) and 235 VE (0.73 eV), is disrupted by a peak that represents a significant mixture of Fe and Ru states. The nonzero DOS values at all Fermi levels suggest metallic character for the $Ti_{9-n}Fe_{2+n}Ru_{18}B_8$ compounds. Furthermore, a local maximum present near these Fermi levels, and arising largely from the Fe 3d orbitals, indicates a possible electronic instability in this system.

The partial DOS curves reveal that states −10 to −7 eV are primarily from boron, viz., 55% of the total states, which then tail off nearly 0% at 0 eV. Ru states are 40% of the total states over the same energy range and increase to 65% of the total states from −5 to −3 eV. The Ru band contribution decreases significantly between −3 and 0 eV, becoming a secondary component for states near 0 eV. Of the remaining states 3−5 eV below the VE count range shown, 20% are Ti states and 10% arise from the Fe atoms. The Fe orbitals increase to a sharp maximum at 230 VE (+0.5 eV) and then decrease rapidly to nearly zero. These states originate primarily from the Fe 'ladders', while states from the Fe 1d sites (original 2b-chains) show a very narrow peak just above 0 eV, close to 228 VE, which corresponds to "$Ti_7Fe_4Ru_{18}B_8$". Above +1.5 eV, Ti and Ru valence d-orbitals dominate the DOS curve with the Ru states tailing off at even higher energy. Consequently, the broad pseudogap-like feature in the total DOS curve stems from an increase of the partially filled Ti bands above the observed VE counts and a decrease of the Ru bands over this same energy range. The peak between 220 and 228 VE arises significantly from Fe-based orbitals.

The spin-polarized total DOS curve, using LSDA, is also shown in Figure 3. Gross features of the spin-polarized (LSDA) and nonspin-polarized (LDA) DOS curves are quite similar except for states near 0 eV. This similarity arises from the preponderance of Ru, B, and Ti orbitals composing the electronic structure. The difference between the two DOS curves is the absence of the Fe-based peak and expression of a deep pseudogap near 0 eV in the spin-polarized curve. This pseudogap appears because the Fe spin orbitals split into a majority spin band, which moves below 0 eV, and a minority spin band, which is largely pushed above 0 eV (see also Figure 3). The observed VE counts for $Ti_{9-n}Fe_{2+n}Ru_{18}B_8$, i.e., 220−228 VE, correspond to Fermi levels that are within the pseudogap once spin-polarization is activated. Furthermore, the Stoner model[16,17] for itinerant magnetism is satisfied in "$Ti_{8.5}Fe_{2.5}Ru_{18}B_8$". In this case, the large Fe-based partial DOS at the Fermi level combined with the exchange-correlation integral determined by Janak[18] for BCC Fe does, in fact, exceed unity. Therefore, the formation of spontaneous magnetic moments at the Fe sites is likely.

Chemical bonding features of $Ti_{9-n}Fe_{2+n}Ru_{18}B_8$ based on "$Ti_{8.5}Fe_{2.5}Ru_{18}B_8$" can be analyzed on the basis of −COHP[14] curves, shown in Figure 4, and their integrated areas, i.e., −ICOHP values. Interatomic distances and −ICOHP values for nearest neighbor contacts in "$Ti_{8.5}Fe_{2.5}Ru_{18}B_8$" are compared to chemical systems having similar environments and distances to elemental metals and listed in Table 4.

The bonding network has been described previously in the analogous $Ti_9Fe_2Ru_{18}B_8$ and $Ti_9M_2Ru_{18}B_8$ (M = Cr, Mn, Co, Ni,

dx.doi.org/10.1021/ja200909r |J. Am. Chem. Soc. 2011, 133, 6832–6840

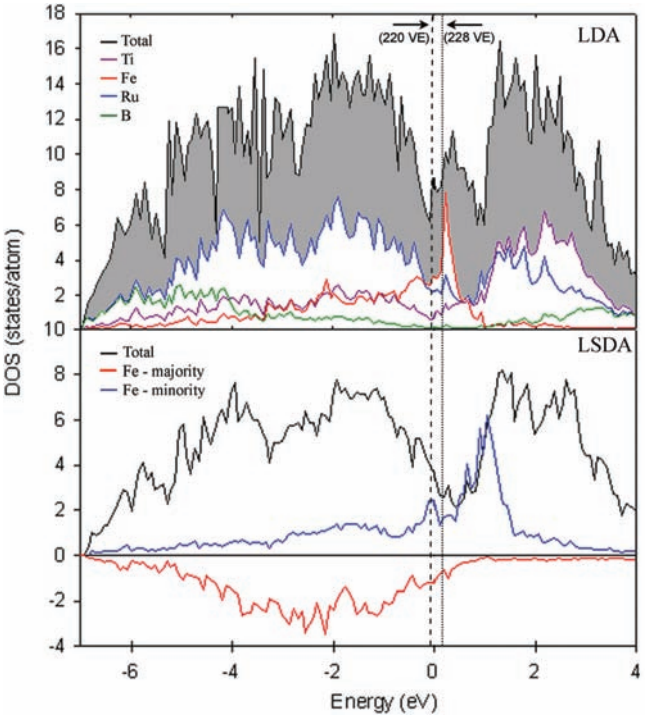

Figure 3. (Top) Total and partial DOS curves using LDA for "$Ti_{8.5-}Fe_{2.5}Ru_{18}B_8$" ($n$ = 0.5; 222 VE). The total DOS is scaled by a factor of 4 for clarity. (Bottom) Total DOS curves using LSDA (black) is overlaid with two partial Fe DOS curves, majority spin (red) and minority down (blue). The reference energy, 0 eV, is set for 222 VE.

Cu, Zn) to contain an extensive Ru−B interaction.[5,21] The structure also shows a substantial metallic bonding network consisting of Ru−Ru, Ti−Ru, and Ru−Fe interactions. The most substantial contributors are the early transition metal (Ti)−late transition metal (Ru) orbital interactions, which have been described by Brewer.[22] Ti atoms in the cubic prisms (2b- and 4h-chains) have a strong interaction with the surrounding Ru atoms with an −ICOHP value of 2.22 eV/bond, which is similar to the value calculated for CsCl-type TiRu, which also shows similar interatomic Ti−Ru distances. Ti−Ru interactions for Ti atoms sitting in the pentagonal prisms (4h and 8j sites) have longer lengths and correspondingly smaller −ICOHP values.

The −COHP curves for averaged Ru−Ru, Ti−Ru, Ru−Fe, and Ru−B interactions reveal that the upper bound of VE counts for $Ti_{9-n}Fe_{2+n}Ru_{18}B_8$ is largely controlled by Ti−Ru and, to lesser extents, by Ru−Fe and Ru−B orbital interactions. Averaged Ti−Ru interactions are optimized almost precisely at 228 VE, a valence electron count appropriate for "$Ti_7Fe_4Ru_{18}B_8$". Since the averaged Ru−Ru and Ru−Fe interactions are noticeably antibonding at this VE count, and Ru−B interactions are nonbonding, the maximum Fe content, which will lead to the highest VE count in $Ti_{9-n}Fe_{2+n}Ru_{18}B_8$ is ca. n = 2, which is in good agreement with experiment.[8]

Another factor influencing the observed range of VE counts in $Ti_{9-n}Fe_{2+n}Ru_{18}B_8$ includes states associated with the Fe1-ladders and the 3d metal 2b-chains. The ligand field splitting of these Fe atomic orbitals was determined through a 'fatband' analysis of the bands between −1.5 and 1.5 eV, the results of which are illustrated in Figure 5. The 3d orbitals of each Fe atom at the 1d sites (original 2b-chains), which are located within square prisms of Ru atoms, are split into the nearly triply degenerate xy, yz,

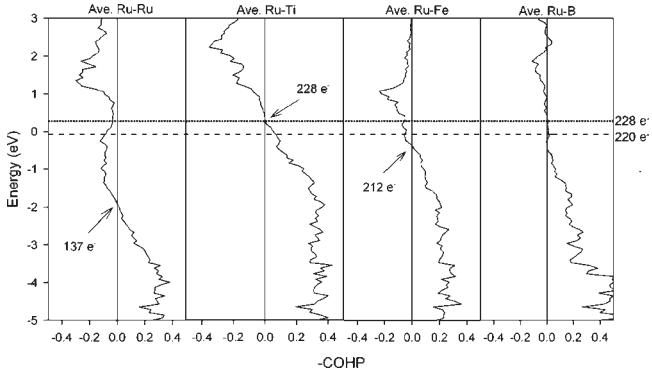

Figure 4. Averaged spin polarized −COHP curves for the nearest neighbor heteroatomic and homoatomic contacts in "$Ti_{8.5}Fe_{2.5}Ru_{18}B_8$" ($n$ = 0.5). The reference energy (0 eV0 is set to 222 VE. The dashed and solid lines, respectively, correspond to 220 VE and 228 VE, which are the lower and upper bounds of observed VE counts in $Ti_{9-n}Fe_{2+n}Ru_{18}B_8$.

Table 4. Various Interatomic Distances and Associated −ICOHP Values in "$Ti_{8.5}Fe_{2.5}Ru_{18}B_8$" and Related Binary Compounds and Elemental Metals

bond	distances (Å)	−ICOHP (eV/bond)
Ru−Ru	2.670−2.852	0.58−1.19
Ru−Ru (hcp)	2.651−2.708	1.45−1.69
Ru−Ti (pentagonal prism)	2.807	1.48
Ru−Ti (cubic prism)	2.578	2.22
Ru−Ti (CsCl-type)[19]	2.656	1.97
Ru−Fe	2.520−2.858	0.52−1.65
Ru−B	2.151−2.204	2.70−2.72
Ru−B ($Ru_{11}B_8$)[20]	2.057−2.245	2.78
Fe1−Fe1	2.497	1.04
Fe1−M2	3.010	0.66
Fe−Fe (BCC)	2.483	1.53

and xz atomic orbitals (b_2 + e wave functions in C_{4v} site symmetry) lower in energy than the nearly doubly degenerate z^2 and $x^2 - y^2$ atomic orbitals (a_1 + b_1 wave functions). The nearly degenerate energetic disposition of these orbitals reflects the nearly cubic field of the eight nearest neighbor Ru atoms surrounding each 1d Fe atom site. Furthermore, the experimental VE counts fall exactly in the gap of these ligand field split 3d orbitals. The 3d orbitals forming the Fe1-ladder have net Fe−Fe bonding interactions in the dimer with the σ, δ, and π^* dimer orbitals lowest in energy, followed by the δ^* orbital, and then π^*, δ^*, and σ^* orbitals highest in energy. The symmetrically equivalent near neighbor Fe1−Fe1 (dimer) interaction results in a band dispersion over a wide energy range, spreading the π^* interaction across the energy window shown, whereas the π bonding interactions of the dimer are found primarily below the energy window examined, perturbed by the surrounding Ru orbitals, which lie in an orientation that make them likely to interact these orbitals of the Fe1-ladder. Interestingly, the observed VE counts fall almost exclusively within the band of δ^* interactions of the Fe1−Fe1 dimer. Thus, the range of observed $Ti_{9-n}Fe_{2+n}Ru_{18}B_8$ phases are influenced by both the robust Ti−Ru and Ru−B interactions as well as the ligand field splitting of the 3d orbitals at the magnetically active Fe atoms.

dx.doi.org/10.1021/ja200909r |J. Am. Chem. Soc. 2011, 133, 6832–6840

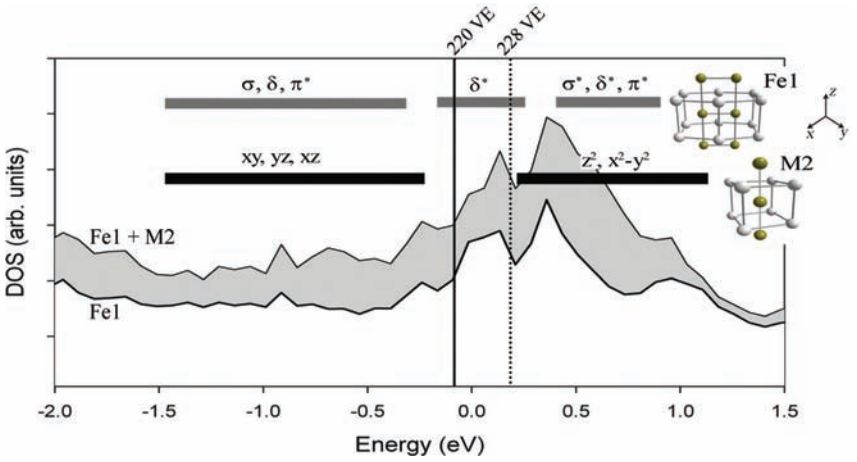

Figure 5. Partial DOS (LDA) of the Fe1-ladder and Fe2 (2b-chain) of "$Ti_{8.5}Fe_{2.5}Ru_{18}B_8$" ($n$ = 0.5) with the corresponding ligand field splitting of the separate coordination environments superimposed as lines indicating band widths. The splitting pattern was determined using a 'fatband' analysis of the electronic band structure.

Table 5. Calculated Total Magnetic Moments and Local Magnetic Moments (given as μ_B/atom) at the 3d Metal Sites Containing Fe Atoms for Models of "$Ti_{9-n}Fe_{2+n}Ru_{18}B_8$" ($n$ = 0, 0.5, 1, 2, 3) According to Table [1,a]

		magnetic moment (μ_B)						
n	VE count	total	2b-chain (M3)		4h-chain (M2)		4h-ladder (Fe1)	
n = 0	220	8.90	Ti	0.00	Ti	0.00	Fe	2.24
n = 0.5	222	13.5	Ti	0.00	Ti	0.00	Fe	2.23
			Fe	2.23				
n = 1	224	14.1	Fe	2.24	Ti	0.00	Fe	2.26
n = 2	228	21.1	Ti	0.00	Fe	2.34	Fe	2.53
n = 3	232	26.8	Fe	2.24	Fe	2.37	Fe	2.60

[a] For these calculations, the WS radii, respectively, of Ti and Fe are 1.62 Å and 1.45 Å.

The Fe atoms and their orbital interactions also influence the magnetic behavior of the $Ti_{9-n}Fe_{2+n}Ru_{18}B_8$ system. Resolving the total DOS from these Fe orbitals into majority and minority spin bands shows substantial spin-polarization (see Figure 3) and large local magnetic moments at each Fe site. The ground-state magnetic ordering of "$Ti_{8.5}Fe_{2.5}Ru_{18}B_8$" was determined to be ferrimagnetic, i.e., an antiferromagnetic interaction between the Fe1-ladder site and the 1d site is 2 meV/formula unit lower in energy than a ferromagnetic interaction after convergence. The magnetic moment on the Fe1-ladder site is 2.23 μ_B/Fe while the moment at the 1d site is antiparallel to the Fe1-ladder with a magnitude 2.23 μ_B/Fe. These magnetic moments at Fe atoms also induce moments on the surrounding Ru atoms, ranging from −0.02 to 0.13 μ_B/Ru (the sign of the moment is given with respect to that of the Fe1-ladder). The moments of the Ru atoms nearest to the Fe atoms order parallel to Fe, while all other Ru atom moments order antiparallel. The Ti and B atoms hold very small local moments, ranging from −0.01 to −0.06 μ_B/Ti atom and −0.01 to 0 μ_B/B atom.

Magnetic Ordering in $Ti_{9-n}Fe_{2+n}Ru_{18}B_8$. As mentioned above, the magnetization of $Ti_{9-n}Fe_{2+n}Ru_{18}B_8$ samples arises primarily from the Fe sites with some polarization of nearest neighbor Ru sites. A summary of the local Fe magnetic moments calculated for "$Ti_{9-n}Fe_{2+n}Ru_{18}B_8$" ($n$ = 0, 0.5, 1, 2, 3) is presented in Table 5.

The calculated local magnetic moment for the isolated Fe1-ladder in $Ti_9Fe_2Ru_{18}B_8$ is 4.48 μ_B/Fe_2-dimer, with the Ti atoms in the two 'chain' sites carrying negligible moments. Substituting Fe atoms for Ti atoms in the "isolated" 2b-chain (M3) sites (see Figure 1) does not affect the theoretical moment at the 'ladder' site, while the additional Fe atoms exhibit a local moment of 2.23 μ_B/Fe. However, the incorporation of Fe atoms at the 4h-chain (M2) sites, which forms the 'scaffold' structure with the 'ladder,' creates a calculated magnetic moment that is 0.1 μ_B/Fe larger than in the 2b-chains. Interestingly, the 'ladder' portion of the 'scaffold' has a significantly larger magnetic moment of 5.06 μ_B/Fe_2. In fact, the substitution of Fe atoms at sites with near neighbor Fe atoms tends to result in larger magnetic moments than when the Fe atoms occupy isolated sites. As a result, with small incorporations of Fe atoms, e.g., as in "$Ti_{8.5}Fe_{2.5}Ru_{18}B_8$", one may expect a minimal change in the measured magnetic moment based on the site preference for the 2b-chain site. With greater Fe content, e.g., as in "$Ti_7Fe_4Ru_{18}B_8$", the measured magnetic moment should increase because substitution at the 4h-chain site will lead to a considerable increase in Fe content, an enhanced local moment from substitution at the 4h-chain, and the amplified magnetic moment in the 'ladder'. In fact, preliminary experimental data show the measured magnetic moment in $Ti_8Fe_3Ru_{18}B_8$ is smaller than that of $Ti_9Fe_2Ru_{18}B_8$, whereas the initial data show the measured moment in $Ti_7Fe_4Ru_{18}B_8$ is much larger.[8] Although these models explain the increase in moment for $Ti_7Fe_4Ru_{18}B_8$, it does not explain the decrease in moment for $Ti_8Fe_3Ru_{18}B_8$. Therefore, a more complete analysis

dx.doi.org/10.1021/ja200909r |J. Am. Chem. Soc. 2011, 133, 6832–6840

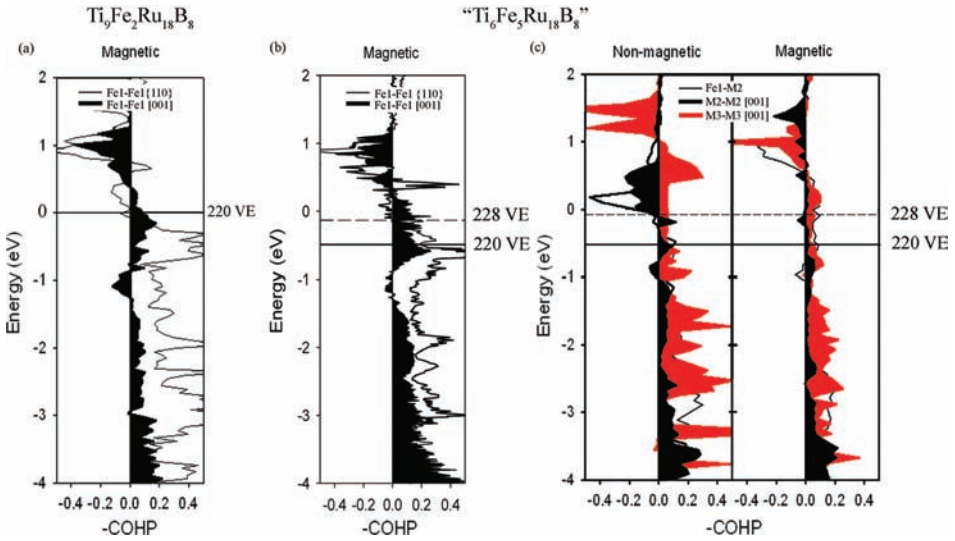

Figure 6. (a) The −COHP (LSDA) curves of the Fe1−Fe1 (ladder) interactions in $Ti_9Fe_2Ru_{18}B_8$. (b) The −COHP (LSDA) curves of the Fe1−Fe1 (ladder) interactions in "$Ti_6Fe_5Ru_{18}B_8$" ($n = 3$). (c) The −COHP (LDA, left, and LSDA, right) curves of the Fe1 (ladder)−M2 (4h-chain), M2−M2, and M3−M3 interactions. The second two contacts are along the [001] direction. The solid line identifies the Fermi level for 220 VE; the dashed line identifies the Fermi level for 228 VE.

of magnetically ordered models in $Ti_{9-n}Fe_{2+n}Ru_{18}B_8$ must be established.

First, we will investigate possible magnetic structures through an analysis of the magnetic and nonmagnetic −COHP curves using the "$Ti_6Fe_5Ru_{18}B_8$" ($n = 3$) model in which the 2b- and 4h-chain sites contain Fe atoms. In this instance, we invoke the rigid-band approximation from the Fe-rich side, an approximation that is reasonably validated by the DOS curves shown in Figure 2. The substitution at the 4h-chain site results in the formation of a tetramer of Fe atoms along the {110} directions, and that in the [001] direction forms an extended 'scaffold' structure (see Figure 1b). The central two atoms of the 'scaffold', which formerly made up the 'rungs' of the Fe ladders (Fe1−Fe1), have nearly identical −COHP curves to the previously reported $Ti_9Fe_2Ru_{18}B_8$ along both the {100} and [001] directions,[5] which are shown in Figure 6a and 6b. The −COHP curves for the Fe1−M2 interactions, making up the outside of the 'scaffold', as well as the M2−M2 interactions along the [001] direction, are all illustrated in Figure 6c. In the nonspin polarized case, Fe1−M2 interactions are nearly optimized, while the M2−M2 interactions along [001] show an occupation of antibonding states between 220 and 228 VE. M3−M3 interactions along the [001] direction, however, have bonding states occupied for the same (observed) VE counts.

Spin polarization affects these orbital interactions, moving the optimized interactions for Fe1−M2 and M3−M3 contacts well above 228 VE and creating M2−M2 nonbonding states occupied over the range 220−228 VE. At a given VE count, the occupation of antibonding states between magnetically active atoms has been previously described to indicate ferromagnetic ordering, whereas when nonbonding or bonding states between magnetic atoms are occupied, antiferromagnetic coupling is preferred.[6,7,23] Therefore, from the −COHP curves presented in Figure 6c, along the [001] direction the magnetic moments at the M2 and M3 sites should order, respectively, ferromagnetically and antiferromagnetically. Furthermore, the Fe1−M2 interaction along {110} should be ferromagnetic.

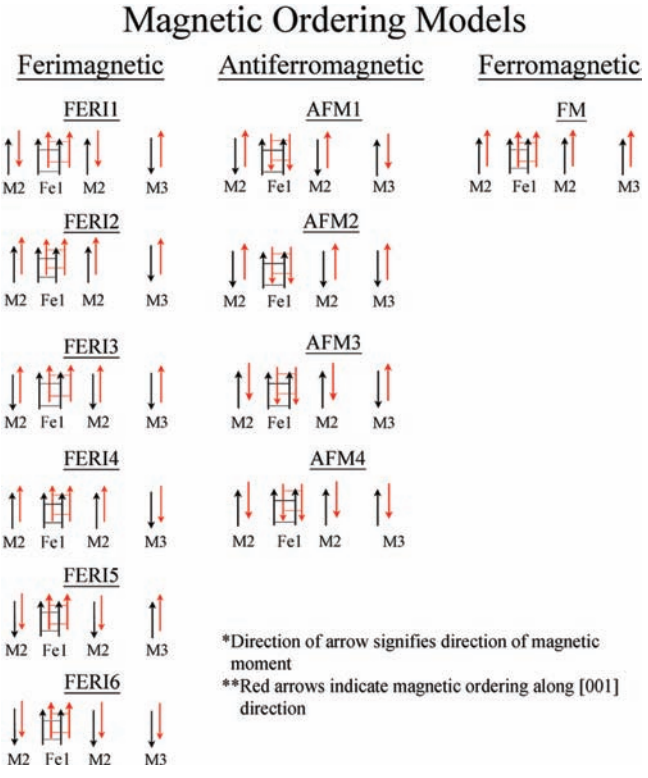

Figure 7. Magnetically ordered models of "$Ti_6Fe_5Ru_{18}B_8$" ($n = 3$) with arrows indicating the orientations of the magnetic moments for the Fe1 (ladder), M2 (4h-chain), and M3 (2b-chain) sites. The two different colors signify two different unit cells along the [001] direction. The sizes of all arrows are arbitrary.

Clearly, there are numerous magnetic exchange paths in $Ti_{9-n}Fe_{2+n}Ru_{18}B_8$ for $n > 0$. Using −COHP curves to predict magnetic exchange will only be useful for through-space interatomic interactions, as in Fe1−M2, M2−M2, and M3−M3 contacts. Long-range, through-bond interactions cannot be

assessed by this technique. As we mentioned earlier, the Ru atoms that are nearest neighbors with the magnetically active Fe atoms will be polarized. Therefore, long-range Fe1−M3 and M2−M3 magnetic coupling can exist in $Ti_{9-n}Fe_{2+n}Ru_{18}B_8$. To determine such long-range magnetic ordering, one ferromagnetic (FM), six ferrimagnetic (FERI), and four antiferromagnetic (AFM) models of "$Ti_6Fe_5Ru_{18}B_8$" (n = 3) were constructed by varying the initial local moments on the three inequivalent Fe sites, i.e., Fe1, M2, and M3, and allowing the calculations to converge self-consistently. These models are depicted schematically in Figure 7. Then, using a rigid band approximation, the total energies were calculated for the range of VE counts, i.e., 220−230 VE, by integrating the total DOS for each magnetic model to the desired electron count with Simpson's integration method.[24] The magnetic moments of the most magnetically active elements, i.e., all Fe atoms and their nearest neighbor Ru atoms, were calculated using the differences between the IDOS values of the majority and minority spin bands at the desired valence electron counts.

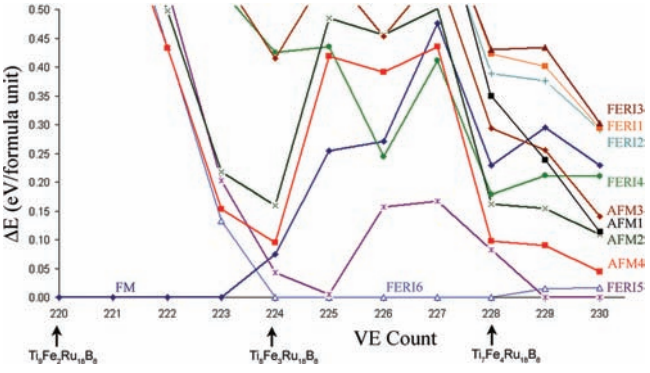

Figure 8. Relative total energies vs VE count for the various magnetically ordered models of "$Ti_{9-n}Fe_{2+n}Ru_{18}B_8$". The lowest energy model is given as 0.00 eV; VE counts range from 220 VE ($Ti_9Fe_2Ru_{18}B_8$) to 230 VE ("$Ti_{6.5}Fe_{4.5}Ru_{18}B_8$").

A graph of the valence electron count versus the total energy, relative to the lowest energy model at each VE count, is plotted in Figure 8 with the full energy range provided in Supporting Information. The resulting magnetic moments for each lowest energy case are listed in Table 6.

At low VE counts and, therefore, low Fe content (220−222 VE), the most favorable model is FM by at least 400 meV/formula unit. Although this prediction of magnetic order arises from a rigid band approximation applied to "$Ti_6Fe_5Ru_{18}B_8$", it does follow the experimental findings of ferromagnetic ordering in $Ti_9Fe_2Ru_{18}B_8$.[5] The total calculated magnetic moment at 220 VE, however, is much larger than the calculated using $Ti_9Fe_2Ru_{18}B_8$, i.e., 12.75 μ_B for "$Ti_6Fe_5Ru_{18}B_8$" (n = 3) versus 5.1 μ_B[5] for $Ti_9Fe_2Ru_{18}B_8$. The larger estimated total moment arises from the elevated concentration of Fe site potentials in "$Ti_6Fe_5Ru_{18}B_8$" (n = 3) and the lower spin polarization associated with Ti valence states. However, the local magnetic moments on the individual Fe atoms are slightly smaller than in the parent structure.[5]

A magnetic ordering transition occurs from FM to FERI6 at 224 VE, flipping the moments of the chain site atoms (M2 and M3) from parallel to antiparallel with respect to the Fe1 'ladder'. The most favorable model between 224 and 228 VE is FERI6, with ferromagnetic ordering within the Fe1 'ladder' but antiferromagnetic ordering between the Fe1 'ladder' and the 4h-chain (M2) sites, making a ferrimagnetic 'scaffold'. Over this range of VE counts, the total moment is low and nearly constant, within 0.1 μ_B because the magnetic moments of both the M2 and M3 sites are antiparallel to the Fe1 'ladders'. Moreover, there is a substantial polarization of the Ru sites closest to the Fe1 'ladders,' a polarization which is antiparallel to the ladder site moments and further lowers the total calculated moment. Experimentally, an initial analysis of the experimental magnetic data for $Ti_8Fe_3Ru_{18}B_8$ (224 VE) has a measured magnetic moment that is smaller than $Ti_9Fe_2Ru_{18}B_8$,[5] which likely stems from ferrimagnetic ordering. The theoretical prediction of the FERI6 model for this electron count fits the data well. In this case the opposing spins of

Table 6. Favored Magnetically Ordered Models as a Function of VE Count for $Ti_{9-n}Fe_{2+n}Ru_{18}B_8$ Based on a Rigid Band Approximation of the DOS of "$Ti_6Fe_5Ru_{18}B_8$" (n = 3)[a]

		magnetic moment (μ_B/atom)						
VE count	favored model	total moment (μ_B/f.u.)	4h-ladder (Fe1)	4h-chain (M2)	2b-chain (M3)	Ru (Fe1)	Ru (M2)	Ru (M3)
220	FM	12.75	2.28	2.20	2.23	0.18	0.14	0.09
221	FM	12.78	2.27	2.19	2.22	0.19	0.15	0.09
222	FM	12.82	2.28	2.19	2.21	0.20	0.15	0.09
223	FM	12.92	2.28	2.17	2.19	0.21	0.16	0.09
224	FERI6	1.61	−2.16	2.12	2.14	0.43	0.02	−0.06
225	FERI6	1.45	−2.17	2.09	2.14	0.51	−0.01	−0.06
225	FERI5	3.08	2.21	−2.06	2.19	−0.08	0.09	0.01
226	FERI6	1.50	−2.16	2.07	2.13	0.51	−0.01	−0.06
227	FERI6	1.52	−2.15	2.04	2.13	0.51	−0.00	−0.06
228	FERI6	1.51	−2.13	2.02	2.12	0.51	−0.00	−0.07
229	FERI5	3.64	2.20	−1.98	2.19	−0.12	0.11	0.01
229	FERI6	1.47	−2.12	2.00	2.11	0.52	−0.00	−0.07
230	FERI5	3.54	2.20	−1.98	2.19	−0.12	0.10	0.01
230	FERI6	1.48	−2.11	2.03	2.09	0.52	−0.00	−0.07

[a] When two models are listed, their energy difference is less than 50 meV/formula unit. The local magnetic moments (in μ_B/atom) are derived using the corresponding IDOS values of the spin-polarized calculations. The signs of the magnetic moments represent parallel (+) or antiparallel (−) to the moments at the M3 sites. The Ru atoms are labeled by the nearest magnetic atom.

dx.doi.org/10.1021/ja200909r |J. Am. Chem. Soc. 2011, 133, 6832–6840

the M2 and M3 sites with respect to the ladder site would result in an overall lower magnetic moment, which is in excellent agreement with the preliminary experimental data.

Further addition of valence electrons to 229 and 230 VE shows two probable magnetic models, FERI6 and FERI5, which both containing a ferrimagnetic 'scaffold' and are separated by ca. 15 meV/formula unit. The difference between these two models is the magnetic ordering of the 2b-chain (M3) with respect to the 4h-chain (M2), which is, respectively, parallel and antiparallel to each other in FERI6 and FERI5. The distance between the 2b-chain (M3) and the 4h-chain (M2) sites is ca. 6.5 Å, which is sufficiently long that through-space exchange is small, but that through-bond using bridging Ru sites is necessary. In FERI5, there is greater polarization of Ru sites closest to M2 than to M3, which affects these relative energies. Finally, the total magnetic moment of the FERI5 models is larger than the FERI6 models because of preferred parallel magnetic ordering of the M3 moments with respect to the moments at the Fe1 'ladder'.

For the range of compounds in $Ti_{9-n}Fe_{2+n}Ru_{18}B_8$ that have been obtained synthetically, i.e., $n = 0$, 1, and 2, the predictions of magnetic structures and trends in total magnetic moments, presented in Table 6 and Figure 8, coincide well with experimental observations. The models with the higher electron counts, e.g., $Ti_7Fe_4Ru_{18}B_8$ (228 VE), do begin to differ from the experimental findings, but this is likely due to changes which stem from differences in mixed Ti/Fe occupancies at the M2 and M3 sites. The effect of atomic mixing on long-range magnetic ordering is currently under investigation.

CONCLUSIONS

We have presented the theoretical electronic structures of "$Ti_{9-n}Fe_{2+n}Ru_{18}B_8$" ($n = 0$, 0.5, 1, 2, 3), which pertain to the substituted intermetallic borides, $Ti_{9-n}Fe_{2+n}Ru_{18}B_8$ ($n = 1$, 2).[8] The total DOS curves reveal a pseudogap at the corresponding Fermi levels, while invoking spin polarization results in the formation of large, localized magnetic moments at the Fe atoms and some polarization induced at the neighboring Ru atoms. An analysis of −COHP curves shows a bonding network similar to those described in $Ti_9Fe_2Ru_{18}B_8$ and $Ti_9M_2Ru_{18}B_8$ (M = Cr, Mn, Co, Ni, Cu, Zn).[5,21] Through an analysis of site energies and bond energies, Ti/Fe mixing may occur at both the 2b- and 4h-chain sites in $Ti_{9-n}Fe_{2+n}Ru_{18}B_8$. Moreover, Fe substitution at the 4h-chain (M2) sites, which creates magnetic scaffolds, increases the local moments at the Fe1-'ladder' sites. The electronic structure of the model "$Ti_{8.5}Fe_{2.5}Ru_{18}B_8$" ($n = 0.5$) provided a detailed description of the chemical bonding features in the $Ti_{9-n}Fe_{2+n}Ru_{18}B_8$ series and identified two important factors regulating the observed VE counts to lie between 220 and 228: (i) optimized Ti−Ru orbital interactions; (ii) ligand field splitting of Fe 3d orbitals in the Fe1-'ladders' and 2b-chain (M3) sites. A rigid band approximation, which is reasonably valid over the observed range of VE counts, predicted ferromagnetic behavior at low Fe content, i.e., $n \leq 0.75$ in $Ti_{9-n}Fe_{2+n}Ru_{18}B_8$, but complex ferrimagnetic behavior at higher Fe content, i.e., $n > 0.75$, in agreement with experiment.

ASSOCIATED CONTENT

Supporting Information. Tables of the empty sphere locations, Wigner−Seitz radii, "$Ti_6Fe_5Ru_{18}B_8$" IDOS values using the rigid band approximations, and figures including the composition-dependent LDA−DOS curves and the full energy range of the VE count versus total energy. This material is available free of charge via the Internet at http://pubs.acs.org.

AUTHOR INFORMATION

Corresponding Author
gmiller@iastate.edu

ACKNOWLEDGMENT

The authors acknowledge the generous financial support through a joint grant provided by the National Science Foundation (USA; NSF DMR 05-02671, 08-06507) and the Deutsche Forschungsgemeinschaft (Germany) through the Materials World Network program.

REFERENCES

(1) Eibenstein, U.; Jung, W. *Z. Anorg. Allg. Chem.* **1998**, *624*, 802.
(2) Nagelschmitz, E. A.; Jung, W. *Chem. Mater.* **1998**, *10*, 3189.
(3) Nagelschmitz, E. A.; Jung, W.; Feiten, R.; Müller, P.; Lueken, H. *Z. Anorg. Allg. Chem.* **2001**, *627*, 523.
(4) Fokwa, B. P. T.; Lueken, H.; Dronskowski, R. *Chem.—Eur. J.* **2007**, *13*, 6040.
(5) Fokwa, B. P. T.; Samolyuk, G. D.; Miller, G. J.; Dronskowski, R. *Inorg. Chem.* **2008**, *47*, 2113.
(6) Landrum, G. A.; Dronskowski, R. *Angew. Chem., Int. Ed.* **1999**, *38*, 1389.
(7) Landrum, G. A.; Dronskowski, R. *Angew. Chem., Int. Ed.* **2000**, *39*, 1560.
(8) Goerens, C.; Brgoch, J.; Miller, G. J.; Fokwa, B. P. T. *Inorg. Chem.* **2010**submitted for publication.
(9) Brgoch, J.; Yeninas, S.; Prozorov, R.; Miller, G. J. *J. Solid State Chem.* **2010**, *183*, 2917.
(10) Andersen, O. K. *Phys. Rev. B* **1975**, *12*, 3060.
(11) Andersen, O. K.; Jepsen, O. *Phys. Rev. Lett.* **1984**, *53*, 2571.
(12) Krier, G.; Jepsen, O.; Burkhardt, A.; Andersen, O. K. *TB-LMTO-ASA Program*, 4.7 ed., Stuttgart, Germany, 1995.
(13) von Barth, U.; Hedin, L. *J. Phys. C* **1972**, *5*, 1629.
(14) Dronskowski, R.; Blöchl, P. E. *J. Phys. Chem.* **1993**, *97*, 8617.
(15) Miller, G. J. *Eur. J. Inorg. Chem.* **1998**, 523.
(16) Stoner, E. C. *Proc. R. Soc. London A* **1936**, *154*, 656.
(17) Stoner, E. C. *Proc. R. Soc. London A* **1938**, *165*, 372.
(18) Janak, J. F. *Phys. Rev. B* **1977**, *16*, 255.
(19) Raub, E.; Roeschel, E. *Z. Metallkd.* **1963**, *54*, 455.
(20) Aselius, J. *Acta Chem. Scand.* **1960**, *14*, 2169.
(21) Fokwa, B. P. T.; Goerens, C.; Gillessen, M. *Z. Kristallogr.* **2010**, *225*, 180.
(22) Brewer, L. *Science* **1968**, *161*, 115.
(23) Dronskowski, R.; Korczak, K.; Lueken, H.; Walter, J. *Angew. Chem., Int. Ed.* **2002**, *41*, 2528.
(24) Atkinson, K. *An Introduction to Numerical Analysis*; 2nd ed.; John Wiley & Sons: New York, 1989.